Unusually high-affinity Mg2+ binding at the AU-rich sequence within the antiterminator hairpin of a Mg2+ riboswitch

Korth, M M T ; Sigel, Roland K O

Abstract: Mg2+-Responsive riboswitches represent a fascinating example of bifunctional RNAs that sense Mg2+ ions with high selectivity and autonomously regulate the expression of Mg2+-transporter proteins. The mechanism of the mgtA riboswitch is scarcely understood, and a detailed structural analysis is called for to study how this RNA can selectively recognize Mg2+ and respond by switching between two alternative stem loop structures. In this work, we investigated the structure and Mg2+-binding properties of the lower part of the antiterminator loop C from the mgtA riboswitch of Yersinia enterocolitica by solution NMR and report a discrete Mg2+-binding site embedded in the AU-rich sequence. At the position of Mg2+ binding, the helical axis exhibits a distinct kink accompanied by a widening of the major groove, which accommodates the Mg2+-binding pocket. An unusually large overlap between two adenine residues on the opposite strands suggests that the bending may be sequence-induced by strong stacking interactions, enabling Mg2+ to bind at this so-far not described metal-ion binding site.

DOI: https://doi.org/10.1002/cbdv.201200031

Unusually High-Affinity Mg^{2+} Binding at the AU-Rich Sequence within the Antiterminator Hairpin of a Mg^{2+} Riboswitch

by **Maximiliane M. T. Korth** and **Roland K. O. Sigel***

Institute of Inorganic Chemistry, University of Zürich, Winterthurerstrasse 190, CH-8057 Zürich (phone: +41 44 635 4652; fax: +41 44 635 6802; e-mail: roland.sigel@aci.uzh.ch)

Mg^{2+}-Responsive riboswitches represent a fascinating example of bifunctional RNAs that sense Mg^{2+} ions with high selectivity *and* autonomously regulate the expression of Mg^{2+}-transporter proteins. The mechanism of the *mgtA* riboswitch is scarcely understood, and a detailed structural analysis is called for to study how this RNA can selectively recognize Mg^{2+} and respond by switching between two alternative stem loop structures. In this work, we investigated the structure and Mg^{2+}-binding properties of the lower part of the antiterminator loop C from the *mgtA* riboswitch of *Yersinia enterocolitica* by solution NMR and report a discrete Mg^{2+}-binding site embedded in the AU-rich sequence. At the position of Mg^{2+} binding, the helical axis exhibits a distinct kink accompanied by a widening of the major groove, which accommodates the Mg^{2+}-binding pocket. An unusually large overlap between two adenine residues on the opposite strands suggests that the bending may be sequence-induced by strong stacking interactions, enabling Mg^{2+} to bind at this so-far not described metal-ion binding site.

Introduction. – Gen regulation systems have evolved to fulfill the cell's requirement for optimal levels of protein production at all times. An intricate network of corresponding processes responds to the cell's ever changing demands throughout the cell cycle. Protein-based control mechanisms have long been acknowledged to modulate gene expression, whereas the role of RNA-based regulation is still emerging. Small untranslated RNA nucleotides can selectively silence genes by interfering with their target mRNA [1]. While RNA interference is still mediated by protein factors, single-stranded antisense RNAs can directly undergo base pairing to a complementary target sequence in a mRNA and modulate its expression [2]. The regulatory function of RNA in a riboswitch sequence is more complex. Riboswitches are *cis*-acting elements that control the expression of the downstream transcript [3]. Located in the 5′-untranslated region (5′-UTR) of mRNAs, they serve as specific targets for RNA-binding metabolites or cofactors. Usually, the protein encoded in the downstream gene is involved in the biosynthesis or the transport of the recognized ligand and thus able to fine-tune its intracellular concentration. Upon binding of the regulating metabolite, the riboswitch sequence undergoes a structural rearrangement that modulates gene expression either on the transcriptional or on the translational stage [4][5]. Specific Mg^{2+} recognition by bacterial riboswitch sequences has only recently been reported. To date, two Mg^{2+}-sensing riboswitches in bacterial cells are known, the *mgtA* riboswitch, which regulates the expression of the Mg^{2+} transporter MgtA and was first discovered in *Salmonella enterica*, and the 'M-box' riboswitch, which was studied in the 5′-UTR of the *mgtE* gene in *Bacillus subtilis* [6][7]. In this study, we concentrate on the *mgtA* riboswitch.

The Mg^{2+} homeostasis in *Salmonella enterica* is governed on two levels. The cell is able to respond to the extracellular Mg^{2+} concentration by a two-component regulatory system, PhoP and PhoQ, that controls the expression of the Mg^{2+} influx mediators, MgtA and MgtB, at the transcription-initiation step [8]. In 2006, a riboswitch sequence in the 5′-UTR of the *mgtA* gene was discovered that senses the intracellular Mg^{2+} level and can autonomously regulate the expression of MgtA at the transcription-elongation step [6]. In the proposed regulation mechanism, alternative base pairing of distinct parts of the sequence allows the 5′-UTR to switch between two predicted stem loop structures (*Fig. 1*).

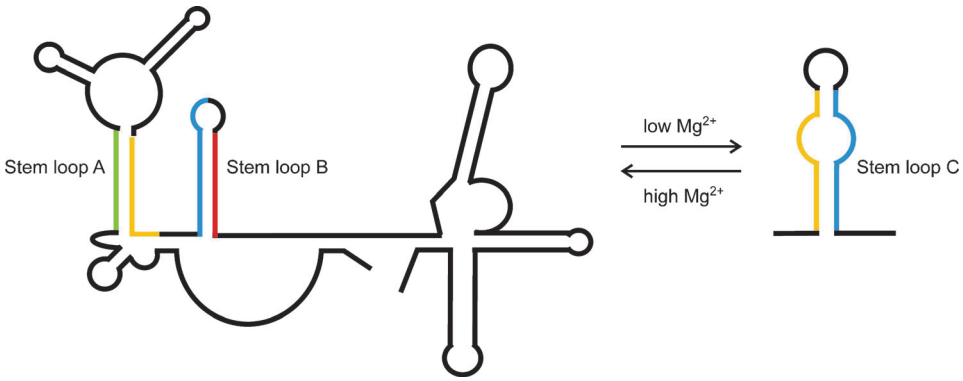

Fig. 1. *Schematic view of the mgtA 5′-UTR illustrating the Mg^{2+}-induced switch.* By pairing the green part of the sequence to the yellow, and the blue part to the red, stem loops A and B are formed at high Mg^{2+} concentration. At low Mg^{2+} concentration, alternative base pairing of the yellow to the blue part rearranges the 5′-UTR to form the antiterminator stem loop C.

Down regulation of mgtA at high Mg^{2+} concentration is achieved by formation of stem loops A and B. As a direct consequence, transcription is stalled before the coding region of the gene is reached. Stem loop C serves as an anti-terminator, promoting the transcription of the full-length gene at low Mg^{2+} concentration. An investigation of the microbial genome database revealed six more species with *mgtA* homologs, in which the gene was preceded by sequences that share the ability to adopt the alternative stem-loop structures A and B *vs.* C in the transcript [6]. This phylogenetic conservation supports the proposed model and emphasizes the importance of the functional roles assigned to the stem loops. Two very recent publications independently reported the discovery of a proline-rich open reading frame, termed *mgtL*, which is embedded in the riboswitch sequence and seems to influence the *mgtA* regulation in a translation-coupled manner. The exact role of the *mgtL* open reading frame in the regulation of the *mgtA* riboswitch nevertheless remains a matter of debate [9][10]. Additionally, it was suggested that enhanced degradation of the transcript plays a part in the regulation, *i.e.*, the riboswitch targets the transcript for RNAse E cleavage [11].

The mechanism by which the RNA specifically recognizes the Mg^{2+} level and accordingly arranges its secondary structure into either one of the mutually exclusive stem loops is not understood, and information about the selectivity in recognition of different metal ions by nucleic acids is at the moment very limited [12–16]. Probing the

structure of large RNAs by chemical and enzymatic methods as reported for the *mgtA* riboswitch can provide local information on single- or double-stranded sites, but neither information on the detailed three-dimensional structure nor on metal-binding sites and affinities can be obtained [6].

In our study, we address this problem by investigating a single stem loop of the *mgtA* riboswitch and its Mg^{2+}-binding properties by NMR. Detection of Mg^{2+} coordination to nucleic acids by NMR is challenging, as this ion is spectroscopically silent, and its binding is kinetically labile; therefore, this ion does not necessarily occupy a fixed coordination site [12][17][18]. Nevertheless, detailed information on the solution structure and complete assignment of the proton resonances allows monitoring the effects of Mg^{2+} coordination on the chemical shifts and the resonance line widths to obtain insight on binding sites and affinities [17–21]. According to the switching model proposed by *Groisman* and co-workers, stem loop C serves as an anti-terminator loop that promotes *mgtA* transcription and is favored at low Mg^{2+} concentration [6]. That stem loop C formation is required for the transcription of the full-length gene was supported by the fact that mutations affecting the formation of stem loop C render the cell unable to express the *mgtA* gene at all and emphasizes its importance [6]. The nucleotides making up the base pairing in stem loop C are highly conserved over the above mentioned six microbial species, and feature a similar pattern of GC and AU stretches of two to four nt length in the helical part [6]. As Mg^{2+} is expected to bind to sequence-specific sites within the *mgtA* riboswitch, the binding affinities of these alternate GC and AU motives can give a first hint towards the mechanism of Mg^{2+} recognition by the riboswitch. The stem loop C sequence from *Yersinia enterocolitica* turned out to be a promising starting point for our NMR investigations as it is *in vitro* transcribed in high yields and gives well-resolved spectra. In this report, we present the solution structure of a shortened stem loop C (designated 'loop C short') construct and reveal a high Mg^{2+} affinity site which is located in the major groove of the lower stem. Here, the RNA forms a notable negatively charged binding pocket that coincides with a kink in the helical axis.

Results and Discussion. – *Spectral Features of Loop C and Loop C Short.* The predicted secondary structure of the stem loop C sequence as found in the *mgtA* 5′-UTR of *Y. enterocolitica* comprises a helix of eleven base pairs, which is topped by a region of two bulges and a closing pentaloop (*Fig. 2*). The two bulges and the loop are separated by two GC base pairs, respectively [6]. An additional AU closing base pair is also possible which would result in a three-membered loop. This base pairing is probably not very strong, as a closing GC base pair generally stabilizes a loop better than an AU pair, and a pentaloop is formed preferentially with respect to a three-membered terminal loop [22][23].

We transcribed a construct of the full-length stem loop C sequence with the addition of 5′-GGA as a starting sequence to increase transcription yield [24]. The initial [^{1}H,^{1}H]-NOESY spectrum of the stem loop C construct recorded in D_2O shows a rather crowded sequential walk region. Starting from the 5′-end, the sequential walk could be followed throughout the helical part of stem C but not beyond the first bulge. The [^{1}H,^{1}H]-NOESY spectrum in H_2O displays 14 strong signals for the imino protons of all the *Watson–Crick* base pairs of the lower helix as well as the GU wobble pair (*Fig. 3*).

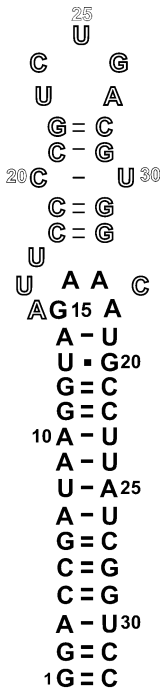

Fig. 2. *Sequence and secondary structure of the loop C and loop C short constructs.* Loop C short comprises the lower helix of the loop C topped with a GAAA tetraloop. The nucleotides of the loop C short construct are represented in solid black letters. The numbering scheme in solid black letters applies to the loop C short construct and is used in the text even when referring to the full-length construct.

Some additional weak signals are observed that indicate less stable base pairings in the upper part of the stem loop. The signals of an U connected by a cross-peak to a G were assigned to U23 and G22 in the upper part of the full-length construct.

The J_{HNN}-COSY experiment allows to observe a coupling across a N–H···N H-bond and thus to directly correlate base-pairing residues [25][26]. Cross-peaks are observed for the five AU base pairs in the lower part of the helix, but no signals for the closing AU below the first bulge and the closing AU in the loop, again indicating that these AU pairs are not properly formed (*Fig. 3*,*a*). The GC base pairs show only very weak coupling across the H-bond, but the existence of the NOE connectivities between guanine imino and cytosine amino protons across the strands confirm the formation of the respective base pairs. Following the pattern of the imino cross-peaks between the two strands, the imino resonances for the helical part could be unambiguously assigned in the 2D experiment.

To assign the resonances of all non-exchangeable protons and obtain NOE distance restraints for the helical part, we designed a truncated construct that consists of the lower helix closed with a GAAA tetraloop. This loop C short construct gives well-resolved spectra that could be fully assigned and integrated to derive the necessary NOE distance restraints for structure calculation. The sequential walk of the helix as well as the assignment of the imino resonances is in accordance with the spectra obtained for the full-length construct (Fig. S1[1])). In the [^{1}H,^{1}H]-NOESY spectra in

[1]) *Supplementary Material* can be obtained upon request from the authors.

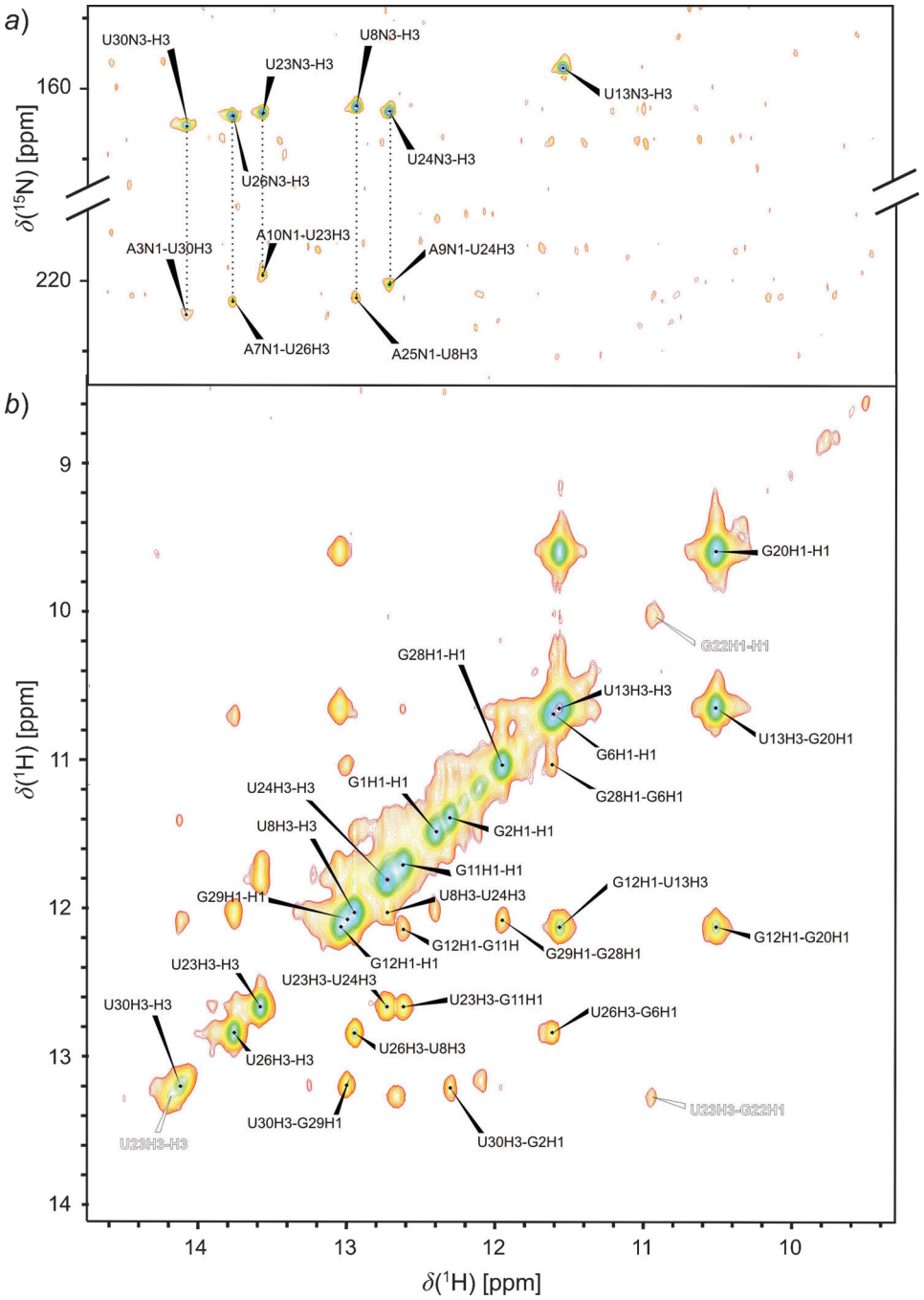

Fig. 3. *Imino resonances of the full-length stem loop C sequence. a*) In the HNN-COSY spectrum, the N(1) of the adenine residues are correlated with the base-pairing uracil N(3) across the H-bond, indicating the formation of five stable AU base pairs within stem loop C. *b*) Sequential assignment of the imino resonances in the helical part below the first bulge was possible in the [^{1}H,^{1}H]-NOESY acquired in H_2O/D_2O 90 : 10, assignments of the upper part beyond the first bulge (G22 and U23) are indicated in red.

D_2O of both, the full-length and the truncated construct, the H2 resonances of A9 and A25 are unusually far upfield-shifted with 6.35 and 6.97 ppm, respectively. These untypical chemical shifts indicate the involvement in strong stacking interactions (*Fig. 4,a*) [27]. The typical resonance pattern of the well-known GAAA tetraloop further supports the formation of a stable hairpin with 14 base pairs including the closing A14–U19, indicated by a visible signal for the U19 H3 imino resonance in H_2O [17][28]. Additionally, a strong imino signal for G15 H1 is observed, which is due to the formation of a sheared GA base pair in the loop and probably also forces the A14–U19 interaction [28].

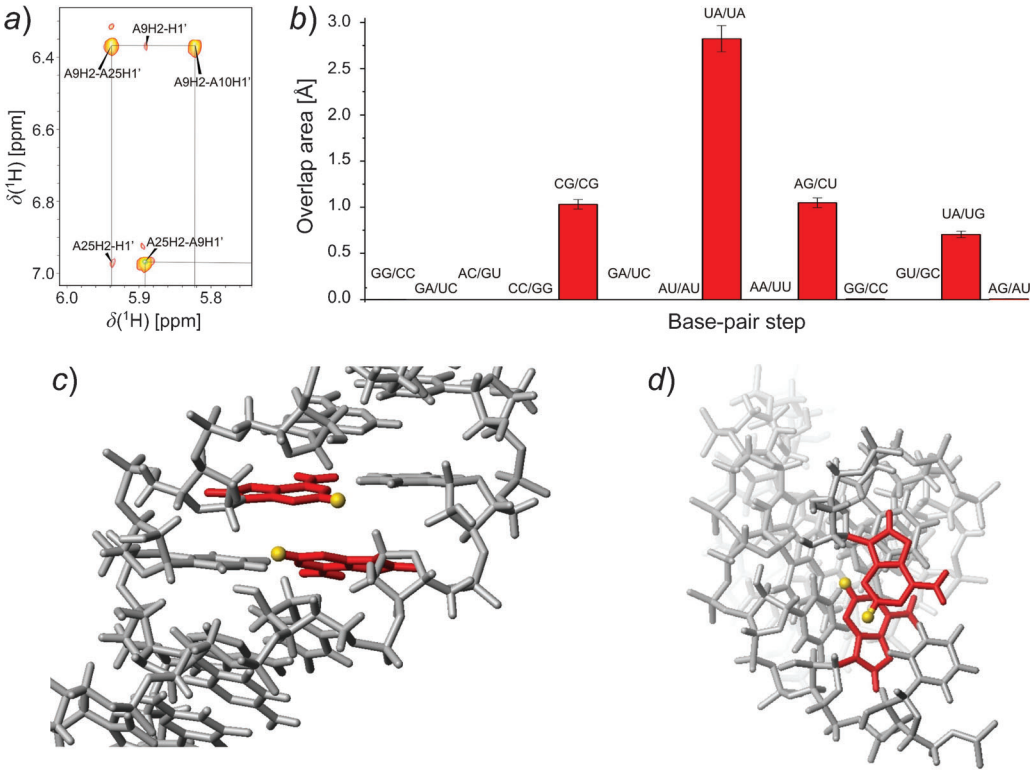

Fig. 4. a) *Section of the [¹H,¹H]-NOESY spectrum of loop C short in D_2O showing the distinct upfield-shifted resonances of A9 H2 and A25 H2 at 6.35 and 6.97 ppm, respectively.* b) *Inter-strand overlap area between each nucleobase of the 5′-helical arm* (G1 to A14) *and the 5′-lying nucleobase on the opposite 3′-arm* (U19 to C32). The average area is zero Å^2, whereas notable overlaps are observed for few base-pair steps, the largest being between A9 and A25. c) *Overlap between A9 and A25 as seen from the side.* The two adenines are colored in red, and their H2 protons are highlighted in gold. d) *The A9/A25 overlap viewed from the top, demonstrating especially the position of A9 H2 above the center of the A25 ring system.*

The Structure of Loop C Short. The structure of loop C short was calculated based on 569 NOE-derived distance restraints (*Table*). The construct forms a stable hairpin with a well-defined helix topped by a GAAA tetraloop. The overall r.m.s.d. of all heavy

atoms amounts to 3.32 ± 1.44 Å averaged over the 20 lowest-energy structures. A closer look at the AU stretch of the lowest-energy structure reveals some interesting features. The helical axis displays a distinct kink that occurs between the AU/AU and UA/UA base pair steps (*Fig. 5*, *a*).

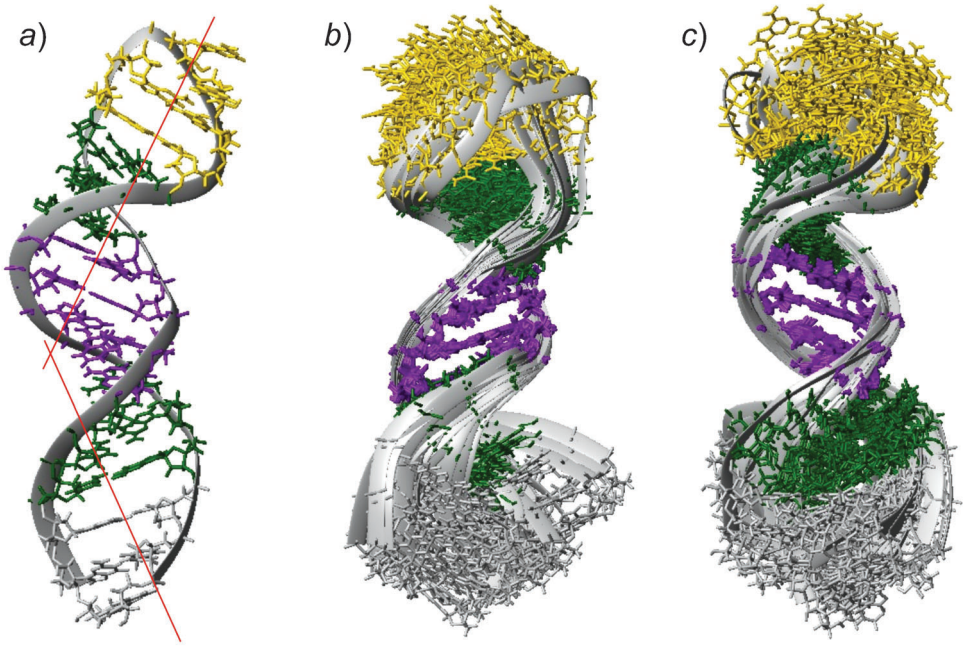

Fig. 5. *Solution structure of loop C short. a*) The lowest-energy structure showing the helical kink at the AU-rich region defined by the two helical axes (red lines) of the lower and the upper part including the loop. *b*) and *c*) Overlay of the 20 lowest-energy structures fitted at the AU stretch.

Table. *Structural Statistics and NMR Restraints for the Structure of Loop C Short.* All statistics are given for the 20 lowest-energy structures out of 200 calculated structures.

NOE-Derived distance restraints	569
Intranucleotide	210
Internucleotide ($\|i-j\|=1$)	201
Long range ($\|i-n\|=2$)	158
Repulsive	0
Dihedral restraints	237
H-Bond restraints	73
R.m.s. Deviations (for all heavy atoms to mean structure) [Å]	
Overall	3.32 ± 1.44
Helix	2.84 ± 1.26
Loop	0.44 ± 0.31
AU stretch	0.68 ± 0.24
NOE Violations > 0.2 Å	0
Dihedral violations $> 5^\circ$	0

Fitting of the heavy atoms of only the AU stretch for all 20 lowest-energy structures gives an r.m.s.d. of 0.68 ± 0.24 Å, indicating that the perceived kink in the helical axis is real and indeed an intrinsic feature of the loop C (*Fig. 5*, *b* and *c*). To analyze the bending of the helical axis within the AU stretch, we compiled the geometrical parameters of each base-pair and each base pair step of the helix for the 20 lowest-energy structures using the 3DNA software [29]. Analysis of the groove width evinces a widening of the major groove at the base pair steps AU/AU and UA/UA. At the same time, the minor groove narrows to a minimum width at the AU/AU step (*Fig. 6*).

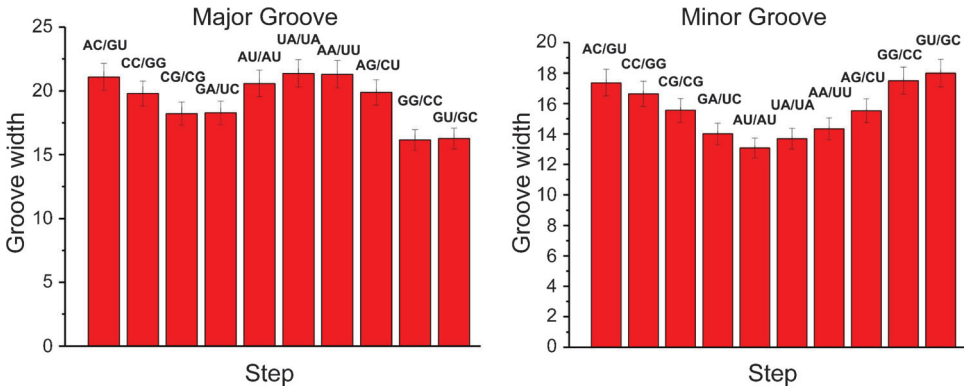

Fig. 6. *Average major- and minor-groove width, defined by cross-strand P–P distances assigned to dinucleotide steps.* The values are calculated based on the method described by *Hassan* and *Calladine* [30], starting at the third base pair from the helix end up to the GU wobble pair below the loop. The error bars refer to the standard deviation from the mean of all 20 lowest-energy structures.

Noticeable in the [^{1}H,^{1}H]-NOESY in D_2O are the large upfield shifts of the H2 resonances of A9 and A25 to 6.35 and 6.97 ppm, respectively (*Fig. 4*, *a*). These unusual chemical shifts can be rationalized by the relative positioning of the two purine bases to each other. The overlap area of successive nucleobases between the opposite strands averaged over the 20 lowest-energy structures discloses a noticeable high value for the adenosines A9 and A25 with almost 3 Å^2 (*Fig. 4*, *b*). This large overlap of A9 and A25 is illustrated by a side view (*Fig. 4*, *c*) and by looking from top along the helical axis (*Fig. 4*, *d*) on the two respective nucleobases. The adenines A9 and A25 are colored in red and the H2 protons are highlighted in gold to demonstrate their position above the center of the aromatic ring system of A25. The large overlap between A9 and A25 evidences a strong stacking interaction between the two adenosines, a finding that is well-known from self-association studies of the parent nucleotide [27][31]. The counter magnetic field on top of the rings induced by the ring current leads to a shielding effect at the two H2 protons of A9 and A25, and explains the exceptionally far upfield shifts of both resonances [27][32].

Mg^{2+} Binding to Loop C Short. Since Mg^{2+} is always associated with RNA stabilizing the 3D structure, mediating interactions with other molecules, and its function in general [13–15][33][34], it is intriguing to find out how the intracellular Mg^{2+} concentration can be precisely and specifically sensed by the *mgtA* riboswitch. Looking at the proposed stem loops individually allows a detailed analysis of their

Mg^{2+}-binding properties. Mg^{2+} Coordination can be followed by NMR, because the chemical shifts as well as the resonance line widths of the nucleic acid protons are affected by a Mg^{2+} binding [35–37].

Chemical-shift changes can result from Mg^{2+} binding in close vicinity to the observed proton, but they can also be due to a Mg^{2+}-induced long-range structural change. Mg^{2+}-Titration experiments in D_2O and chemical-shift mapping analysis of the non-exchangeable protons reveal effects of Mg^{2+} coordination in the helical parts as well as the GAAA tetraloop. Chemical-shift changes of the H1′ and of the aromatic protons appear throughout the whole sequence, the most significant change being 0.2 ppm observed for G2 H8. The observed chemical-shift changes for all H1′ and the aromatic protons H2, H5, H6, and H8 were plotted against the Mg^{2+} concentration. Of the 87 analyzed protons, 62 could be fitted to a 1 : 1 binding isotherm to give estimates of individual binding affinities. The other protons either did not exhibit a significant change in their resonance or could not be traced reliably throughout all ten titration steps. The individual $\log K_A$ values range from 2.44 (A3 H1′) to 4.17 (A3 H2), and appear to be fairly equally spread throughout the sequence with no clustering of especially high or low affinities at a certain region.

To better pinpoint metal-ion binding, we studied the resonance line widths of all protons in loop C short upon titration with Mg^{2+} and Mn^{2+}. The kinetically labile coordination of a Mg^{2+}(aq) ion leads to line broadening of ^1H resonances in close proximity due to its fast exchanging rate. The paramagnetic Mn^{2+} ion causes fast relaxation of nearby nuclear spins, thereby also inducing a line broadening [19][38][39]. As both effects are locally limited to the binding site, they allow a more precise localization of the coordination site than chemical-shift changes [35–37]. Significant line-broadening effects upon addition of Mg^{2+} could be observed for the H8 and H1′ resonances, as well as the imino H1 signals of G1 and G2, pointing to a strong binding of Mg^{2+} at the 5′-terminal phosphate group. Mg^{2+} Binding to the phosphate groups is well-known [13][40–43] and has been quantified with an RNA hairpin of similar size [18]. An additional binding site is indicated in the loop, where the imino resonance of G15 broadens out selectively already at 0.5 mM Mg^{2+}.

Next, we titrated a sample of loop C short with $MnCl_2$, which is commonly used as a mimic for inner-sphere coordination of Mg^{2+} [38]. A selective line broadening at concentrations lower than 250 μM $MnCl_2$ was observed for the imino resonances of G1, G2, G11, and G15 as well as for the H8 resonances of G15 and A16 corroborating the binding sites at the 5′-end and in the loop. Additionally, Mn^{2+} caused a notable line broadening of the H8 resonances of the tandem G11/G12 and the G6/G28/G29 stretch. The imino resonances of these guanines with the exception of G11, however, were not affected. Mn^{2+} Binding to the GAAA tetraloop has been studied previously, and our findings agree with the reported broadening of the G imino resonance of the tetraloop [44][45].

Both the chemical shift mapping analysis and the line broadening studies indicate a strong binding at the 5′-phosphate group, which is expected because of its multiple negative charge. Due to the significant influence of Mg^{2+} binding on the 5′-end, most of the chemical-shift changes of the non-exchangeable protons of the first three residues could not be fitted well enough to give a reliable binding affinity. The same is true for the corresponding base-pairing partners U30–C32. In total, seven $\log K_A$ values for

these six residues were obtained, and they vary between 2.44 (A3 H1′) and 4.17 (A3 H2). At the same time, these two values represent the extremes of $\log K_A$ values obtained within the whole loop C short. In the following GC stretch (C4–G6 and C27–G29, termed *GC1*), the changes in chemical shifts upon Mg^{2+} addition yielded affinity constants around $\log K_A \approx 3.4$, although no line broadening was observed. Nevertheless, metal-ion binding could be corroborated by Mn^{2+} addition, as the peak width of the three GH8 was affected. All non-exchangeable proton resonance shifts of these six residues could be fitted, with the one exception of C5 H5. The middle part of the helix harbors a four-base-pair-long AU stretch, which was already shown to exhibit some interesting structural features. No line-broadening effects upon addition of either Mg^{2+} or Mn^{2+} could be observed for this stretch, indicating that no inner-sphere binding takes place. Nevertheless, the chemical shifts of the protons are strongly affected by Mg^{2+} addition. A third of the non-exchangeable proton shifts could not be fitted reasonably well, but again the variance of the individual $\log K_A$ values within this stretch is relatively small. In accordance with the GC1 region, also in GC2 (G11–U13 and G20–C37), more ^{1}H chemical shifts could be fitted with the signals showing no significant line broadening upon Mg^{2+} addition. Again, Mn^{2+} coordination yielded strong line broadening of the H8 resonances of both G11 and G12. In the loop region, only three of the 17 non-exchangeable protons could not be fitted, and the individual binding affinities show only low variance. The Mg^{2+} binding site in the loop is confirmed by the line-broadening effects observed for the G15 resonances with Mg^{2+} and Mn^{2+}.

The determined $\log K_A$ values do not allow an assignment of distinct metal-ion binding sites within the loop C short RNA, as they do not vary significantly within three times the error limits. M^{2+} Binding to the tetraloop is well-known and corroborated by our data. Mn^{2+} Line broadening indicates binding regions in the two GC regions GC1 and GC2. We decided to assign a further binding region to the central AU stretch because *i*) a majority of non-exchangeable protons exhibits distinct chemical shift changes that could be well fitted, *ii*) the determined $\log K_A$ values agree within their error limits, and *iii*) an effect of the Mg^{2+} bound to the two GC stretches seems unlikely because of the large distance. We divided the stem loop in the two GC stretches GC1 and GC2 (green), the AU stretch (purple), and the loop region (yellow), and calculated the average binding affinities for each region (*Fig. 7*).

When calculating intrinsic affinity constants for different regions within one RNA, one has to be aware that the individual sites compete for Mg^{2+} to about the same extent, as the affinities are all rather similar. Consequently, the amount of Mg^{2+} available to each binding site is less than the total Mg^{2+} concentration due to competition between the individual sites [18][46]. We calculated the intrinsic affinity by an iterative procedure in ten steps using ISTARv2.2 [46]. Like the initial values, also the final individual $\log K_A$ values overlap within their error limits (*Fig. 7* and Table S1[1])). It is intriguing that the final Mg^{2+} affinity constants of the individual regions in this crucial part of the Mg^{2+} sensing riboswitch are by *ca.* 1 log unit higher than generally found in small RNA hairpins, *e.g.*, domain 6 of a group II intron ribozyme [18][46]. This is especially true for the AU stretch, which shows an equivalent affinity towards Mg^{2+} as the two neighboring GC regions. These generally larger affinities are certainly partly due to the lower ionic strength used in the present study

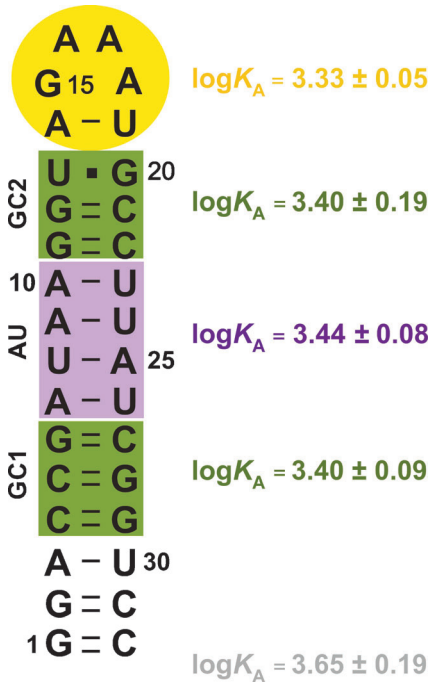

Fig. 7. *The final average binding affinities, log*K_A*, for the respective* Mg^{2+}*-binding regions.* According to the coloring scheme in *Fig. 5*, the AU stretch is shown in purple, the GC stretches in green, and the tetraloop in yellow. The affinity constant shown in grey at the helix end corresponds to the Mg^{2+} affinity to the 5′-terminal triphosphate group.

(50 *vs.* 100 mM KCl). However, we do not expect that this difference in KCl concentration accounts for the total increase in affinity. A further reason is a markedly negatively charged spot embedded in the major groove of the helix at the position of the UA/UA base-pair step (*Fig. 8*) as is revealed by the electrostatic surface potential. The large overlap of the A9 and A25 nucleobases coincides with the accumulation of negative charge. The kinking of the helical axis leads to a widening of the major groove, which exposes the site to the solvent, thereby making it more easily accessible for Mg^{2+} binding. This finding implies an electrostatically driven Mg^{2+} association at the AU stretch in the middle of the stem of loop C short, which is indicated by the high Mg^{2+} affinity found in this region.

Conclusions and Outlook. – A-Form RNA helices feature a deep and narrow major groove, which is disposed to attract positive ions due to a negative electrostatic potential [47]. Sequence-specific localization of cations in the major and minor groove has been proposed to cause a dynamic narrowing of the groove in DNA [48]. A-Tract bending of DNA is known to highly depend on the sequence [49]. An A4T4-containing DNA duplex is bent towards the minor groove at the AT/AT step in the middle, whereas the T4A4-containing molecule shows the opposite behavior and bends towards major groove at the middle TA/TA step [50]. An RNA crystal structure of a

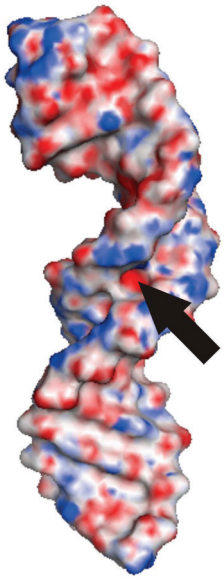

Fig. 8. *Calculated electrostatic surface potential of loop C short.* Red indicates strong negative (-40 kTe^{-1}), white a more neutral (-5 kTe^{-1}), and blue a positive (5 kTe^{-1}) surface charge. The arrow points to the markedly negatively charged spot in the major groove at the AU stretch.

construct consisting of only A and U nucleotides has been reported to feature two notable kinks in the helical axis [51][52]. This intrinsic, sequence-directed curvature might have a functional role in cellular processes. AU-Rich sequences in RNA are mainly found in loop or bulge regions. Within a helix, they might be a recognition motif or a bending point where a double helix is more flexible to accommodate the association with an interaction partner. In addition, single-stranded AU-rich regions are a preferred cleavage site for RNAse E and are found within most mRNAs as also in the 5′-UTR of *mgtA*. Consequently, a release of an AU-rich motif from a secondary or tertiary interaction within the riboswitch might additionally contribute to the regulation mechanism by targeting the 'Mg^{2+}-charged' form for RNAse E cleavage as proposed by *Spinelli et al.* [11].

Phylogenetic sequence conservation is always a strong evidence for the important role of a certain sequence motif. When comparing the stem loop C sequence of the six bacterial *mgtA* 5′-UTRs, an UAA motif can be found in each organism right below the first bulge of the stem loop C. The co-transcriptional translation of the recently discovered proline-rich open reading frame *mgtL*, which is integrated in the *mgtA* riboswitch of *S. enterica*, seems to influence the gene expression geometrically due to the steric demands of ribosome-binding to the sequence [9][10]. The conserved UAA motif corresponds to the stop codon of the 17-residue peptide mgtL, which was found to be essential for the transcription abortion of *mgtA* at high Mg^{2+} in *S. enterica*. The exact mechanism of the *mgtL*-mediated control of *mgtA* transcription and riboswitch activity still remains a matter of debate [9][10].

Even though all three stem loops play an essential part in the function of the *mgtA* riboswitch, the individual stem loops might well undergo tertiary contacts with other parts of the riboswitch to stabilize or destabilize one of the two alternative folds. These tertiary interactions are likely to be Mg^{2+}-dependent and could also proceed in a cooperative fashion as described for the 'M-box' riboswitch [7]. Thus, specific Mg^{2+}-recognition sites and regions of high Mg^{2+} affinity are likely to be spread out over the whole sequence, playing an important role in the switch between the two conformations by stabilizing one fold over the other, or facilitating a favorable transition state. The general, rather high affinity of stem loop C short for Mg^{2+} together with the distinct helix kink at the AU stretch and its Mg^{2+} binding might, therefore, be an important part of the function of the Mg^{2+} specific riboswitch.

Financial support by the *Swiss National Science Foundation* (grant 200021-124834/1to *R. K. O. S.*) and the University of Zurich is gratefully acknowledged. *R. K. O. S.* is a recipient of an ERC Starting Grant 2010.

Experimental Part

General. DNA Oligonucleotides were purchased from *Microsynth* (CH-Balgach), and the nucleotide 5′-triphosphates from *GE Healthcare* (CH-Otelfingen), except UTP, which was obtained from *Acros Organics* (B-Geel). The T7 RNA polymerase used for *in vitro* transcription was home-made [53]. The electroelution apparatus *Biotrap* was from *Schleicher & Schuell* (D-Dassel). For desalting, *VivaSpin Concentrators* (3000 MWCO) from *Sartorius-Stedim biotech* (F-Aubagne) were used. ^{13}C,^{15}N-Labeled RNA was transcribed with isotopically labeled NTPs from *Silantes GmbH* (D-München). $MgCl_2$ for the metal ion titration was obtained as ultrapure soln. (1M) in H_2O from *Fluka-Sigma-Aldrich* [24].

NMR Sample Preparation. Loop C (5′-GGACCGAUAAGGUAAUUCCCCGUCUGACGU-GGCUGCCUUAUCGGUCC) and loop C short (5′-GGACCGAUAAGGUAGAAAUGCCU-UAUCGGUCC) were synthesized by *in vitro* transcription with T7 polymerase from a double-stranded DNA template. All RNA was purified by denaturing 12% PAGE, UV-shadowed, excised from the gel, and recovered by electroelution. After desalting and lyophilization, the sample was dissolved in D_2O (200 µl) containing KCl (50 mM) and EDTA (10 µM) at pH 6.8, adjusted with 5M NaOH. The RNA concentration of the samples varied between 0.24 and 0.8 mM, and was determined on a *Varian Cary 500 Scan* UV/VIS spectrometer by using an extinction coefficient at 260 nm (ε_{260}) of 365.2 mM^{-1} cm^{-1} and 750.2 mM^{-1} cm^{-1}.

NMR Spectroscopy. NMR Spectra were recorded on a *Bruker AV700 MHz* equipped with a CP-TXI *z*-axis pulsed-field gradient cryoprobe. Non-exchangeable proton resonances were assigned from 2D [^{1}H,^{1}H]-NOESY spectra acquired at 303 K (120-ms mixing times), 2D [^{1}H,^{1}H]-TOCSY spectra at 293 K (45-ms mixing time), and [^{13}C,^{1}H]-HSQC spectra, which were recorded separately for the aromatic and the aliphatic range of the ^{13}C resonances. Exchangeable proton resonances were assigned by 2D [^{1}H,^{1}H]-NOESY spectra acquired at 278 K with mixing times of 150 ms and watergate H_2O suppression, and by the aid of a [^{15}N,^{1}H]-HSQC [36][37][54]. The base-pairing scheme was established by a 2D J_{NN}-COSY, correlating the imino N-atoms of uracil (N(3)) and the guanine (N(1)), across the H-bond to the N(1) of adenine or the N(3) of cytosine on the other side of the double helix [55]. All [^{1}H,^{1}H] spectra were recorded with RNA constructs of natural isotope abundance, whereas experiments involving ^{13}C and ^{15}N isotopes were recorded with fully ^{13}C,^{15}N-enriched constructs. NMR Spectra were processed with Topspin2.1 (*Bruker*) and analyzed by using Sparky (http://www.cgl.ucsf.edu/home/sparky/). NOE Peak volumes were integrated with the *Gaussian* peak-fitting function in Sparky.

Structure Calculation. NOE Distances were calculated from the integrated peak volumes obtained from the [^{1}H,^{1}H]-NOESY spectrum acquired at 303 K (120 ms mixing time). Distances were calibrated by using the CALIBA macro in DYANA [56]. The NOEs were grouped into four categories, corresponding to strong (1.8–3 Å), medium (1.8–4.5 Å), weak (3.0–6.0 Å), and very weak (4.0–7.0 Å).

NOEs obtained from [^{1}H,^{1}H]-NOESY peaks in H_2O/D_2O 90:10 were qualitatively assigned as strong, medium weak, or very weak. Sugar pucker restraints were included, based on TOCSY experiments with a 45-ms mixing time [17]. A16 and C32 showed strong H1′/H2′ and H1′/H3′ cross-peaks and were, therefore, restrained to S-type ($\delta = 155 \pm 20°$) A17 and A18 showed medium strong peaks for H1′/H2′ and were left unconstrained. All other nucleotides showed no H1′/H2′ cross-peaks and were, therefore, constrained to N-type ($\delta = 85 \pm 20°$). The other backbone torsion angles (β, γ, and ε) were set to standard A-form in the helical region of the structure. Additional H-bond restraints were added for base pairs whose existence was established by ^{1}H,^{1}H cross-peaks across the helix in the imino region and by HN cross-correlations from the 2D J_{NN}-HNN-COSY experiment [56]. The structure calculations were performed by using CNS1.2 and refined with XPLOR-NIH [57][58]. The 20 structures with the lowest XPLOR energies out of 200 calculated were analyzed by using MOLMOL [59]. The electrostatic surface potential was calculated by using QNIFFT [47] and visualized with PYMOL (*W. L. DeLano*, 2002, http://www.pymol.org).

Mg^{2+}-Titration Studies. The concentration of loop C short in the Mg^{2+} titration experiments was 0.24 mM. Mg^{2+} Binding to loop C short was monitored by observing the line broadening and changes in chemical shifts of the aromatic and the sugar protons in [^{1}H,^{1}H]-NOESY spectra acquired in the presence of 0, 0.25, 0.5, 0.75, 1, 1.5, 2, 2.5, 3, and 4 mM $MgCl_2$ (99.999% D_2O, $I = 0.05$M (KCl), 10 μM EDTA, pH 6.8). In addition, the chemical-shift changes of the imino protons upon addition of Mg^{2+} were monitored by ^{1}H-NMR spectra in the presence of 0, 0.25, 0.5, 0.75, 1, and 1.5 mM $MgCl_2$ (H_2O/D_2O 90:10, $I = 0.05$M (KCl), 10 μM EDTA, pH 6.8).

Mn^{2+} Line-Broadening Experiments. The concentration of loop C short in the line-broadening experiments was 0.3 mM. Mn^{2+} Line broadening of the aromatic and sugar protons resonances was monitored by acquisition of [^{1}H,^{1}H]-NOESY spectra in the presence of 0, 50, 100, 150, 200, and 250 μM $MnCl_2$ (99.999% D_2O, $I = 0.05$M (KCl), 10 μM EDTA, pH 6.8). Line broadening of the imino protons was monitored by recording 1D ^{1}H-spectra in the presence of 0, 10, 20, 50, 100, 150, 200, and 250 μM $MnCl_2$ (H_2O/D_2O 90:10, $I = 0.05$M (KCl), 10 μM EDTA, pH 6.8).

Structure coordinates have been deposited with the *Protein Data Bank* (ID: 2LI4), and the NMR chemical shift assignments have been deposited with the *BioMagResBank* (accession code: 17877).

REFERENCES

[1] G. J. Hannon, *Nature* **2002**, *418*, 244.
[2] C. L. Beisel, G. Storz, *FEMS Microbiol. Rev.* **2010**, *34*, 866.
[3] M. Mandal, R. R. Breaker, *Nat. Rev. Mol. Cell Biol.* **2004**, *5*, 451.
[4] T. M. Henkin, *Genes Dev.* **2008**, *22*, 3383.
[5] R. K. Montange, R. T. Batey, *Annu. Rev. Biophys.* **2008**, *37*, 117.
[6] M. J. Cromie, Y. X. Shi, T. Latifi, E. A. Groisman, *Cell* **2006**, *125*, 71.
[7] C. E. Dann III, C. A. Wakeman, C. L. Sieling, S. C. Baker, I. Irnov, W. C. Winkler, *Cell* **2007**, *130*, 878.
[8] E. A. Groisman, *J. Bacteriol.* **2001**, *183*, 1835.
[9] S.-Y. Park, M. J. Cromie, E.-J. Lee, E. A. Groisman, *Cell* **2010**, *142*, 737.
[10] G. Zhao, W. Kong, N. Weatherspoon-Griffin, J. Clark-Curtiss, Y. Shi, *EMBO J.* **2011**, 1.
[11] S. V. Spinelli, L. B. Pontel, E. García Véscovi, F. C. Soncini, *FEMS Microbiol. Lett.* **2008**, *280*, 226.
[12] E. Freisinger, R. K. O. Sigel, *Coord. Chem. Rev.* **2007**, *251*, 1834.
[13] J. Schnabl, R. K. O. Sigel, *Curr. Opin. Chem. Biol.* **2010**, *14*, 269.
[14] A. M. Pyle, *J. Biol. Inorg. Chem.* **2002**, *7*, 679.
[15] R. K. O. Sigel, A. M. Pyle, *Chem. Rev.* **2007**, *107*, 97.
[16] R. K. O. Sigel, H. Sigel, *Acc. Chem. Res.* **2010**, *43*, 974.
[17] R. K. O. Sigel, D. G. Sashital, D. L. Abramovitz, A. G. Palmer III, S. E. Butcher, A. M. Pyle, *Nat. Struct. Mol. Biol.* **2004**, *11*, 187.
[18] M. C. Erat, R. K. O. Sigel, *Inorg. Chem.* **2007**, *46*, 11224.
[19] S. E. Butcher, F. H.-T. Allain, J. Feigon, *Biochemistry* **2000**, *39*, 2174.

[20] M. C. Erat, O. Zerbe, T. Fox, R. K. O. Sigel, *ChemBioChem* **2007**, *8*, 306.
[21] A. Huppler, L. J. Nikstad, A. M. Allmann, D. A. Brow, S. E. Butcher, *Nat. Struct. Mol. Biol.* **2002**, *9*, 431.
[22] D. R. Groebe, O. C. Uhlenbeck, *Nucleic Acids Res.* **1988**, *16*, 11725.
[23] M. J. Serra, M. H. Lyttle, T. J. Axenson, C. A. Schadt, D. H. Turner, *Nucleic Acids Res.* **1993**, *21*, 3845.
[24] S. Gallo, M. Furler, R. K. O. Sigel, *Chimia* **2005**, *59*, 812.
[25] A. J. Dingley, S. Grzesiek, *J. Am. Chem. Soc.* **1998**, *120*, 8293.
[26] K. Pervushin, A. Ono, C. Fernández, T. Szyperski, M. Kainosho, K. Wüthrich, *Proc. Natl. Acad. Sci. U.S.A.* **1998**, *95*, 14147.
[27] H. Sigel, *Pure Appl. Chem.* **2004**, *76*, 375.
[28] H. A. Heus, A. Pardi, *Science* **1991**, *253*, 191.
[29] X.-J. Lu, W. K. Olson, *Nucleic Acids Res.* **2003**, *31*, 5108.
[30] M. A. El Hassan, C. R. Calladine, *J. Mol. Biol.* **1998**, *282*, 331.
[31] K. H. Scheller, F. Hofstetter, P. R. Mitchell, B. Prijs, H. Sigel, *J. Am. Chem. Soc.* **1981**, *103*, 247.
[32] J. A. N. F. Gomes, R. B. Mallion, *Chem. Rev.* **2001**, *101*, 1349.
[33] S. A. Woodson, *Curr. Opin. Chem. Biol.* **2005**, *9*, 104.
[34] J. K. Frederiksen, R. Fong, J. A. Piccirilli, in 'Nucleic Acid-Metal Ion Interactions', Eds. N. V. Hud, Royal Society of Chemistry, Cambridge, UK, 2009, pp. 260–306.
[35] S. Johannsen, M. M. T. Korth, J. Schnabl, R. K. O. Sigel, *Chimia* **2009**, *63*, 146.
[36] M. C. Erat, R. K. O. Sigel, *Met. Ions Life Sci.* **2011**, *9*, 37.
[37] D. Donghi, R. K. O. Sigel, *Methods Mol. Biol.* **2012**, *848*, 253.
[38] J. Feigon, S. E. Butcher, L. D. Finger, N. V. Hud, *Methods Enzymol.* **2001**, *338*, 400.
[39] M. Pechlaner, R. K. O. Sigel, *Met. Ions. Life Sci.* **2012**, *10*, 1.
[40] E. M. Bianchi, S. A. A. Sajadi, B. Song, H. Sigel, *Chem. – Eur. J.* **2003**, *9*, 881.
[41] H. Sigel, R. Griesser, *Chem. Soc. Rev.* **2005**, *34*, 875.
[42] H. Sigel, E. M. Bianchi, N. A. Corfù, Y. Kinjo, R. Tribolet, R. B. Martin, *Chem. – Eur. J.* **2001**, *7*, 3729.
[43] R. K. O. Sigel, H. Sigel, *Met. Ions Life Sci.* **2007**, *2*, 109.
[44] M. R. Hansen, J. P. Simorre, P. Hanson, V. Mokler, L. Bellon, L. Beigelman, A. Pardi, *RNA* **1999**, *5*, 1099.
[45] S. Rüdisser, I. Tinoco Jr., *J. Mol. Biol.* **2000**, *295*, 1211.
[46] M. C. Erat, J. Coles, C. Finazzo, B. Knobloch, R. K. O. Sigel, *Coord. Chem. Rev.* **2012**, *256*, 279.
[47] K. Chin, K. A. Sharp, B. Honig, A. M. Pyle, *Nat. Struct. Mol. Biol.* **1999**, *6*, 1055.
[48] N. V. Hud, J. Plavec, *Biopolymers* **2003**, *69*, 144.
[49] R. E. Dickerson, *Nucleic Acids Res.* **1998**, *26*, 1906.
[50] R. Stefl, H. H. Wu, S. Ravindranathan, V. Sklenář, J. Feigon, *Proc. Natl. Acad. Sci. U.S.A.* **2004**, *101*, 1177.
[51] A. C. Dock-Bregeon, B. Chevrier, A. Podjarny, J. Johnson, J. S. de Bear, G. R. Gough, P. T. Gilham, D. Moras, *J. Mol. Biol.* **1989**, *209*, 459.
[52] A. C. Dock-Bregeon, B. Chevrier, A. Podjarny, D. Moras, J. S. de Bear, G. R. Gough, P. T. Gilham, J. E. Johnson, *Nature* **1988**, *335*, 375.
[53] P. Davanloo, A. H. Rosenberg, J. J. Dunn, F. W. Studier, *Proc. Natl. Acad. Sci. U.S.A.* **1984**, *81*, 2035.
[54] M. C. Erat, H. Kovacs, R. K. O. Sigel, *J. Inorg. Biochem.* **2010**, *104*, 611.
[55] B. Luy, J. P. Marino, *J. Am. Chem. Soc.* **2000**, *122*, 8095.
[56] P. Güntert, C. Mumenthaler, K. Wüthrich, *J. Mol. Biol.* **1997**, *273*, 283.
[57] A. T. Brünger, P. D. Adams, G. M. Clore, W. L. DeLano, P. Gros, R. W. Grosse-Kunstleve, J. S. Jiang, J. Kuszewski, M. Nilges, N. S. Pannu, R. J. Read, L. M. Rice, T. Simonson, G. L. Warren, *Acta Crystallogr., Sect. D* **1998**, *54*, 905.
[58] C. D. Schwieters, J. J. Kuszewski, N. Tjandra, G. M. Clore, *J. Magn. Reson.* **2003**, *160*, 65.
[59] R. Koradi, M. Billeter, K. Wüthrich, *J. Mol. Graphics* **1996**, *14*, 29; R. Koradi, M. Billeter, K. Wüthrich, *J. Mol. Graphics* **1996**, *14*, 51.

Received January 31, 2012